# L-arginine loading porous PEEK promotes percutaneous tissue repair through macrophage orchestration

Tong Zhao [a,b,1], Xingdan Liu [a,c,1], Zhuangzhuang Chu [a,b], Jing Zhao [b], Dongya Jiang [b], Xiaohua Dong [b], Ziyi Lu [a,b], Kelvin W.K. Yeung [e], Xuanyong Liu [c,d,*], Liping Ouyang [a,b,**]

[a] Laboratory of Key Technology and Materials in Minimally Invasive Spine Surgery, Tongren Hospital, Shanghai JiaoTong University School of Medicine, China
[b] Hongqiao International Institute of Medicine, Tongren Hospital, Shanghai Jiao Tong University School of Medicine, Shanghai, 200336, China
[c] State Key Laboratory of High Performance Ceramics and Superfine Microstructure, Shanghai Institute of Ceramics, Chinese Academy of Sciences, Shanghai, 200050, China
[d] School of Chemistry and Materials Science, Hangzhou Institute for Advanced Study, University of Chinese Academy of Sciences, 1 Sub-lane Xiangshan, Hangzhou, 310024, China
[e] Shenzhen Key Laboratory for Innovative Technology in Orthopaedic Trauma, Guangdong Engineering Technology, Research Center for Orthopaedic Trauma Repair, Department of Orthopaedics and Traumatology, The University of Hong Kong Shenzhen Hospital, Shenzhen, China

## ARTICLE INFO

## ABSTRACT

Infection and poor tissue repair are the key causes of percutaneous implantation failure. However, there is a lack of effective strategies to cope with due to its high requirements of sterilization, soft tissue healing, and osseointegration. In this work, L-arginine (L-Arg) was loaded onto a sulfonated polyetheretherketone (PEEK) surface to solve this issue. Under the infection condition, nitric oxide (NO) and reactive oxygen species (ROS) are produced through catalyzing L-Arg by inducible nitric oxide synthase (iNOS) and thus play a role in bacteria sterilization. Under the tissue repair condition, L-Arg is catalyzed to ornithine by Arginase-1 (Arg-1), which promotes the proliferation and collagen secretion of L929 and rBMSCs. Notably, L-Arg loading samples could polarize macrophages to M1 and M2 in infection and tissue repair conditions, respectively. The results *in vivo* show that the L-Arg loading samples could enhance infected soft tissue sealing and bone regeneration. In summary, L-Arg loading sulfonated PEEK could polarize macrophage through metabolic reprogramming, providing multi-functions of antibacterial abilities, soft tissue repair, and bone regeneration, which gives a new idea to design percutaneous implantation materials.

## 1. Introduction

Percutaneous implantation failure is a worldwide concerned issue. About one million patients are suffering from artificial limb implantation failure worldwide [1,2]. Three reasons account for this issue due to the special environment of percutaneous implants: bacterial infection, soft tissue sealing failure, and inferior hard tissue regeneration. Polyetheretherketone (PEEK) is an FDA-approved implant that can be used clinically as interbody fusion devices, bone implant, spinal fusion devices, etc, due to its good biocompatibility, closed elastic modulus, and

corrosion resistance [3]. In our previous work, sulfonation was applied to construct a porous structure on PEEK surface, and the subsequent works verified that sulfonated PEEK could be a good drug delivery platform due to its superior stability *in vivo* [4–9]. Therefore, it is a good choice to choose PEEK as one of the candidates for percutaneous implantation.

The processes of infected tissue repair include two stages. M1 macrophages are involved in bacterial clearance and killing at the first stage. During the healing process of infected tissue, the activation of early M1 macrophages induces stem cells to secrete acute phase proteins and

activate the complement receptor system. It can help tissues to remove bacteria and other microorganisms [10,11]. Activated M1 macrophages release oxygen-reacting mediators (ROI), nitric oxide (NO), and metalloproteinase-12 (MMP-12), enhancing endocytosis and cooperating with the complement system to effectively kill pathogens [12–14]. However, continued M1 activation would delay or prevent tissue repair. Conversely, M2 macrophages are involved in tissue repair. In the repair stage, M2 macrophages down-regulate the inflammatory response and promote tissue healing by secreting anti-inflammatory factors [15,16]. However, premature activation of M2 would cause fibrosis, resulting in the implantation material being wrapped by fibers, preventing osteoblasts from infiltrating into the material surface, and affecting the tissue integration effect of the material [17,18]. Therefore, according to the characteristics that macrophages play antibacterial and repair roles in sequence [19], the PEEK surface with adaptive response and regulation of macrophage phenotype can achieve clearance and killing of bacteria in the infection stage and promote wound healing in the repair stage.

Changes in metabolic processes play an important role in the regulation of macrophage polarization [20,21]. Infection and injury lead to significant changes in the microenvironment, and induce macrophages to produce bactericidal substances and tissue repair factors to cope with infection and tissue repair by changing their metabolic pathways [22, 23]. Metabolic processes in living organisms are represented by an orderly, continuous variety of chemical reactions. To cope with infection and injury, the body needs to constantly regulate the metabolic direction, flow, and rate of each substance, and change the metabolic pathway of cells. This change process is called metabolic reprogramming. The direction, rate, and flow of reversible reactions during metabolism are mainly affected by three factors: substrate concentration, enzyme activity and product concentration, among which changing substrate concentration is an important way of metabolic reprogramming. Succinate could inhibit the activity of proline hydroxylase (PHD), stabilize the expression of hypoxia inducible factor-1α (HIF-1α), and lead to the accumulation of interleukin-1β (IL-1β), which could promote the polarization of M1 [24]. Derivative metabolites of itaconate and fumarate could inhibit M1 activation through inhibiting IL-1β and NOD-like receptor thermal protein domain associated protein 3 (NLRP3) [25]. Alpha-ketoglutaric acid (α-KG) promotes M2 polarization through a histone demethylase (Jmjd3) dependent pathway [26]. Literatures have disclosed that L-arginine (L-Arg) could inhibit macrophages related inflammation [27]. Li et al. found that Arg carbon dots composite hydrogel could promote M2 polarization through elevating TLR/JAK-STAT-c-Maf axis mediated IL-10 expression. Besides, L-Arg is the substrate of a variety of enzymes to participate in metabolic pathways [28]. Inducible nitric oxide synthase (iNOS) catalyzes L-Arg to NO, inhibiting the tricarboxylic acid (TCA) cycle and thus promoting aerobic glycolysis, and then activates M1 macrophages. L-Arg is hydrolyzed by Arginase-1 (Arg-1) to urea and ornithine, which could be metabolized to polyamine and proline in the next step, thus promoting the TCA cycle and oxidative phosphorylation and inhibiting the NO-mediated inflammatory pathway. The above processes could promote the polarization of M2 macrophages [29,30]. Therefore, loading with L-Arg may achieve bi-directional regulation of macrophage polarization under different situations through metabolic reprogramming.

Consequently, in this work, L-Arg was loaded onto the sulfonated PEEK surface to orchestrate macrophage phenotype through metabolic reprogramming. The sequential macrophage polarization and metabolism reprogramming were detected by immunofluorescent staining and metabolite detection. Both the infected soft healing model and bone defect model were used to study the effect of samples on soft and hard tissue repair. Besides, the mechanisms of samples in macrophage polarization were studied by RNA-Sequence (RNA-Seq) test and Western blot analysis.

## 2. Results

### 2.1. Materials characterizations

PEEK has a smooth surface at high magnification, while sulfonated PEEK (SP) has a uniform three-dimensional (3D) porous structure, which provides a good platform for small molecules loading. After loading with L-Arg, the porous structure is partly covered by the particles. The particles on the surface increase with the elevated L-Arg content. However, with the increase of L-Arg concentration, the agglomeration of material particles becomes obvious (Fig. 1a–e). The results of the contact angle of the sample surface are shown in Fig. 1f. The surface contact angles of L-Arg loading samples are lower than that of PEEK and SP, showing a certain hydrophilicity. Zeta potential curves of PEEK, SP, SPLA5, SPLA10, and SPLA20 samples as a function of pH value are shown in Fig. S1. The Zeta potential of PEEK decreases with the increased pH value, which may be due to the adsorption of hydroxide ions on the surface. The Zeta potential curve of the other four groups changed gently. When pH = 7.4, the Zeta potential trend on the surface of the samples in each group was SPLA5>SPLA10≈SP > SPLA20.

Fourier transform infrared (FTIR) was used to detect the surface groups of the samples, and the results are shown in Fig. 1g. The characteristic peak of L-Arg is found on SPLA5, SPLA10 and SPLA20, and the peak position locates at about 668 cm$^{-1}$. Moreover, the characteristic peak belonging to SP is weakened on SPLA20 because its surface was highly covered by L-Arg. X-ray photoelectron spectroscopy (XPS) was used to further detect the load content of L-Arg. The content of N on SPLA5, SPLA10 and SPLA20 surfaces is about 1.29 %, 2.95 %, and 4.08 %, respectively (Fig. 1h and Fig. S2). The release content of SPLA10 was the highest among these three groups (Fig. 1i).

### 2.2. Macrophage orchestration through metabolic reprogramming

Regeneration along with infection situation occurs hard due to the significant changes in microenvironment, including bacterial membrane debris induced pro-inflammatory cytokines elevation, temperature elevation and metabolism change. At the infection stage, bacteria debris, such as lipopolysaccharides (LPS) and lipoteichoic acid (LTA), activate macrophages to M1 phenotype by iNOS. At the wound healing stage, interleukin-4 (IL-4) induced Arg-1 expression promotes regeneration. Herewith, the pivotal enzymes in different stages are evaluated. LPS and IL-4 were used to mimic the microenvironment of pro-inflammation and anti-inflammation. The co-localized fluorescence of M1 marker (CCR7) and enzyme (iNOS) were evaluated and the results are shown in Fig. 2a and Fig. S3. L-Arg improves iNOS expression, which shows a dose-dependent style. SPLA10 shows an obviously high fluorescent intensity compared to the other four groups due to the highest release content of L-Arg. As SPLA20 has a higher release content of L-Arg than SPLA5, it expresses more iNOS. Interestingly, macrophage polarization shows a reversed regulation style of iNOS. There are more M1 macrophages on SPLA5 surface than SPLA20 and SPLA10. When transformed the stimulation to IL-4, the pivotal enzyme, Arg-1, expressed more in SPLA10 than SPLA5 and SPLA20. M2 polarization exhibits dose dependent style, and fluorescence intensity of CD206 elevated with increased L-Arg release content (Fig. 2b and Fig. S3). Combining observation of CCR7 and CD206 labeled images, it can be found that the intensity of CCR7 and CD206 always exhibits inversed. There are lightest CD206 and darkest CCR7 in SPLA10, while darkest CD206 and lightest CCR7 in SPLA5. In addition, the fluorescent staining about macrophages polarization on samples surface without IL-4 stimulation is performed and the results are shown in Fig. S4. M2 polarization still exhibits L-Arg dose dependent style. However, for M1 polarization, there is no significant difference between PEEK and the groups loading with L-Arg, and SP group has the most M1 macrophage.

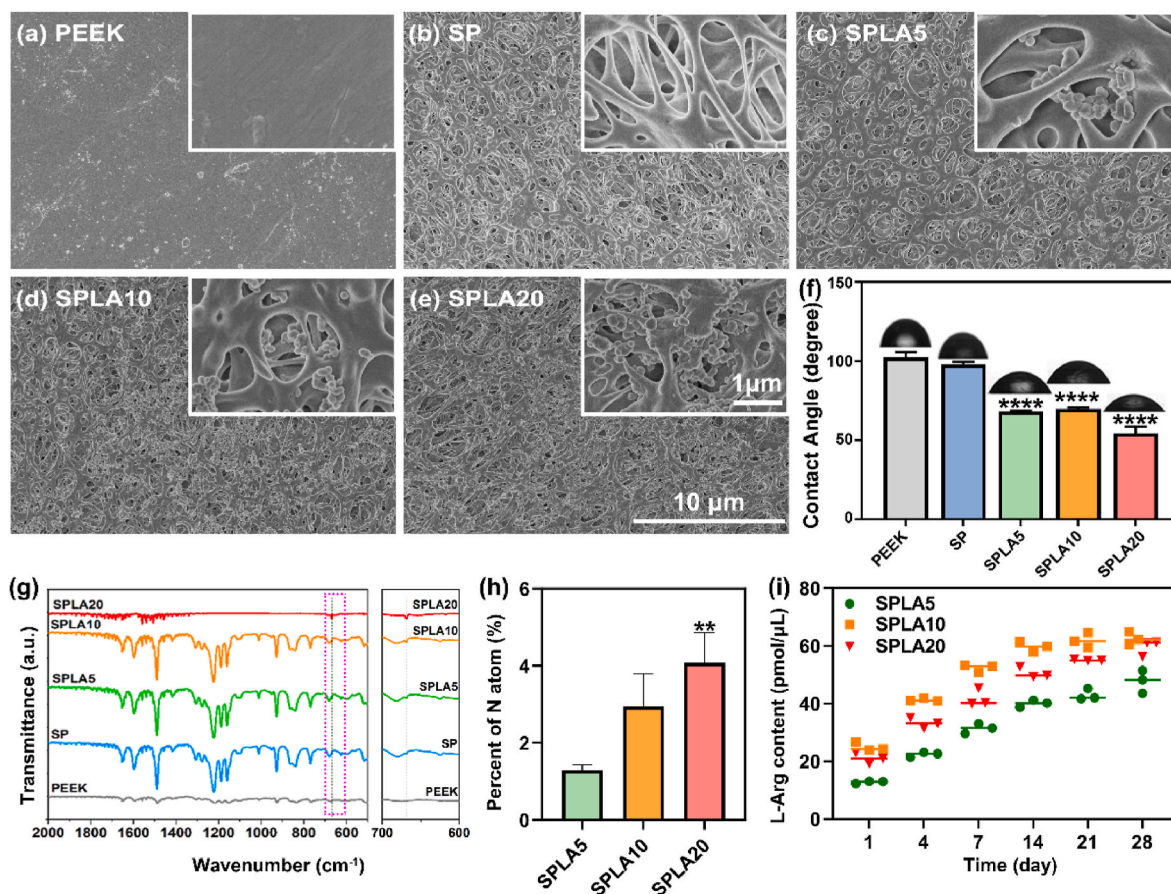iNOS and Arg-1 are the typical enzymes in pro-inflammation and

**Fig. 1. Morphologies and surface properties of the samples.** Surface morphologies of (a) PEEK, (b) SP, (c) SPLA5, (d) SPLA10 and (e) SPLA20; (f) Contact angles of the samples (n = 3); (g) FTIR spectra of the samples; (h) Percent of N atom of the samples tested by XPS (n = 3); (i) L-Arg release of the samples. Data are expressed by mean with SD. Statistical significance was calculated by one-way ANOVA analysis. **p < 0.01 and ****p < 0.0001, compared with PEEK in f and h.

anti-inflammation for catalyzing L-Arg to play bi-functions (Fig. 2c). Under LPS stimulation, iNOS catalyzes L-Arg to produce NO, which could further participate in ROS and antibacterial agent synthesis. While under IL-4 stimulation, IL-4 catalyzes L-Arg to produce ornithine, which is an important source of polyamines and proline to enhance proliferation and collagen secretion. The key downstream productions of L-Arg, NO and ornithine, were detected under different stimulation and the results are shown in Fig. 2d and e. The NO content and ornithine are not affected by the samples themselves without stimuli, which is beneficial for non-infectious situation. However, NO content increased with LPS stimulation, especially in SPLA10 and SPLA20. The effect of L-Arg on NO increase is abolished when applied IL-4 stimulation. Ornithine expression in SPLA10 group is higher than the other four group under IL-4 stimulation. In summary, SPLA10 orchestrates macrophage polarization through metabolism reprogramming. In detail, SPLA10 is metabolized to NO and ornithine to play superior bi-functions of bacteria sterilization and tissue repair through regulating iNOS and Arg-1 expression with LPS and IL-4 stimulation.

### 2.3. Antibacterial abilities

The immuno-antibacterial abilities of the samples *in vitro* were detected and the results are shown in Fig. 3. Macrophages act on intracellular bacteria through metabolites and phagocytosis, and the results are shown in Fig. 3a and b. As the figures show, the number of dead bacteria in the groups loaded with L-Arg is more than that in the PEEK group, and the samples loaded with L-Arg could also promote macrophages to phagocytose bacteria. The effects of SPLA10 on bacteria sterilization and phagocytosis are particularly significant among the five

groups (Fig. S5). The effect of L-Arg loading sulfonated PEEK on *E. coli* is similar to *S. aureus* (Figs. S6 and S7). The intracellular ROS staining of macrophages cultured on the samples for 1 day is shown in Fig. S8. The PEEK group exhibits the lowest intracellular ROS content among the five groups, and SPLA10 group has the highest intracellular ROS content in the L-Arg loading group. Fig. 3c shows the fluorescence staining of intracellular ROS in macrophages cultured on samples for 4 days. PEEK group has the lowest intracellular ROS content among the five groups, and SPLA10 group has the highest intracellular ROS content in the L-Arg loading group, which is conducive to killing intracellular phagocytic bacteria. The results of quantitative ROS content are consistent with the results of fluorescence staining (Fig. S9). ROS content increases significantly in L-Arg loading group compared with PEEK group after culture for 4 days, and the highest ROS content was found in SPLA10 group due to its highest L-Arg release.

### 2.4. In vitro cell response

Ornithine participates in M2 polarization to produce polyamines and proline thus promoting cell proliferation and collagen secretion. As mouse-derived epithelioid fibroblasts (L929) and rat-derived bone marrow mesenchymal stem cells (rBMSCs) are the main cells that affect soft and hard tissue regeneration, the Alarma Blue assay and immuno-fluorescent staining were used to detect the proliferation and collagen secretion of these two types of cells, and the results are shown in Fig. 4. The proliferation of L929 cultured on SP and L-Arg loading SP are both significantly higher than PEEK, however, there are not any discernible difference between SP and SPLA5, SPLA10 and SPLA20 (Fig. 4a). L929 was co-cultured with Raw264.7 and the collagen-III (Col-III) expression
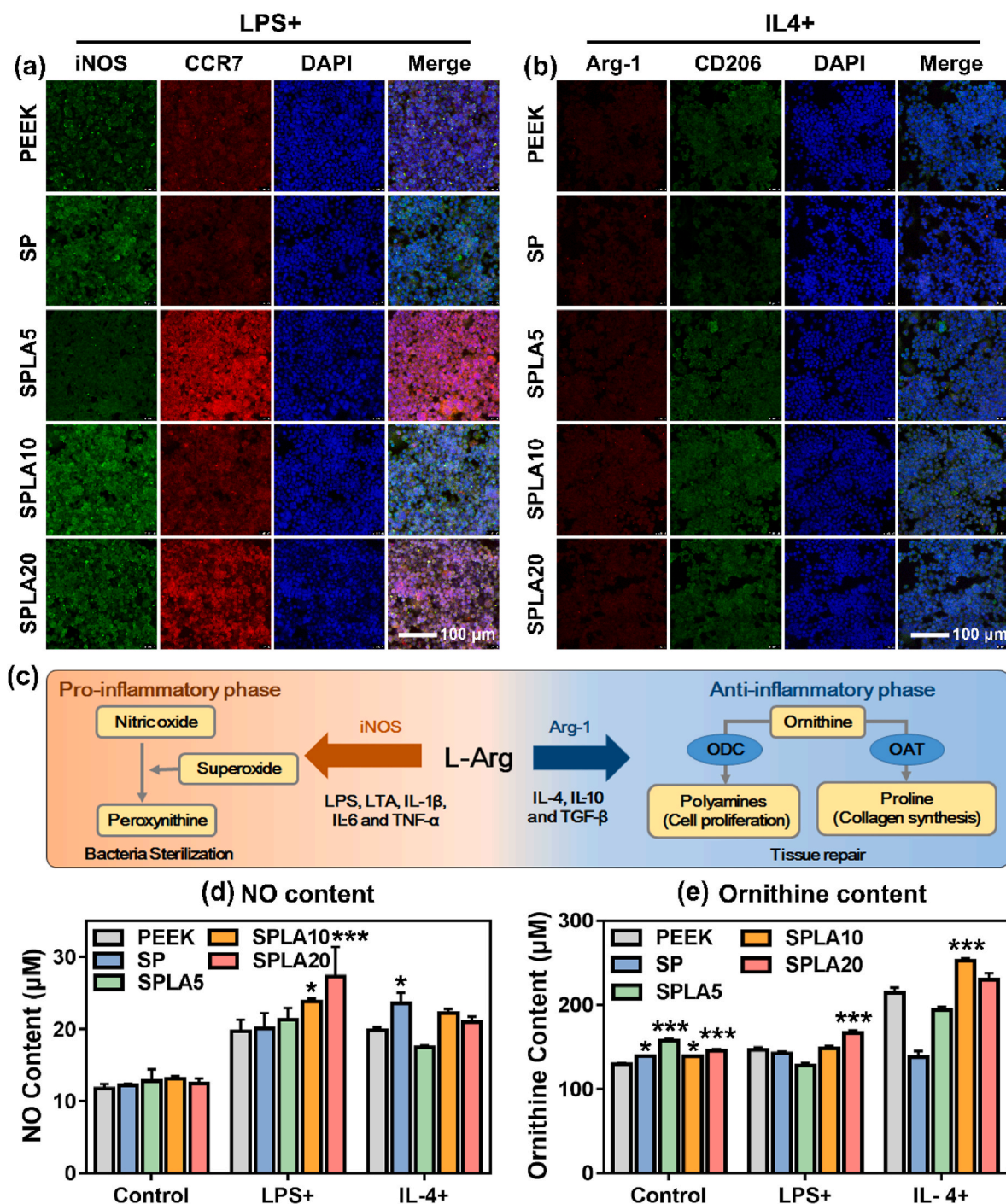
**Fig. 2. Metabolic reprogramming effect of macrophages cultured on L-Arg loading SP.** (a) Co-localized of CCR7 and iNOS of macrophages cultured on PEEK, SP, SPLA5, SPLA10 and SPLA20 surface stimulated by LPS; (b) Co-localized of CD206 and Arg-1 of macrophages cultured on PEEK, SP, SPLA5, SPLA10 and SPLA20 surface stimulated by IL-4; (c) Schematic diagram of L-Arg metabolism in different microenvironment; (d) NO content releasing from macrophages cultured on samples with different stimulations (n = 3); (e) Ornithine content producing from macrophages cultured on samples with different stimulations (n = 3). Data are expressed by mean with SD. Statistical significance was calculated by two-way ANOVA analysis and Tukey's multiple comparison tests. *$p < 0.05$, **$p < 0.01$ and ***$p < 0.001$, compared with PEEK in d and e.

was determined by immunofluorescent staining (Fig. 4b). The cells cultured on SPLA10 surface exhibit more green fluorescence, which proves that its Col-III expresses higher than the other four groups. The green fluorescence on SP is similar to SPLA5 and SPLA20, but all three groups loading with L-Arg are obviously lighter than PEEK. The quantitative average optical density of green fluorescence also shows that SPLA10 exhibits significantly higher than the other four groups, especially for PEEK (Fig. 4c).

Unlike L929, L-Arg loading sulfonated PEEK can significantly promote the proliferation of rBMSCs after culture for 7 days (Fig. 4d). The promotion effect presents L-Arg release dose dependence. SPLA10 exhibits the highest cell proliferation enhancement due to its highest release content of L-Arg. SPLA20 slightly reduces the cell activity compared to SPLA10, possibly due to the high L-Arg loading content on its surface. The immunofluorescent staining and the relative quantitative average optical density of green fluorescence both show that Col-II
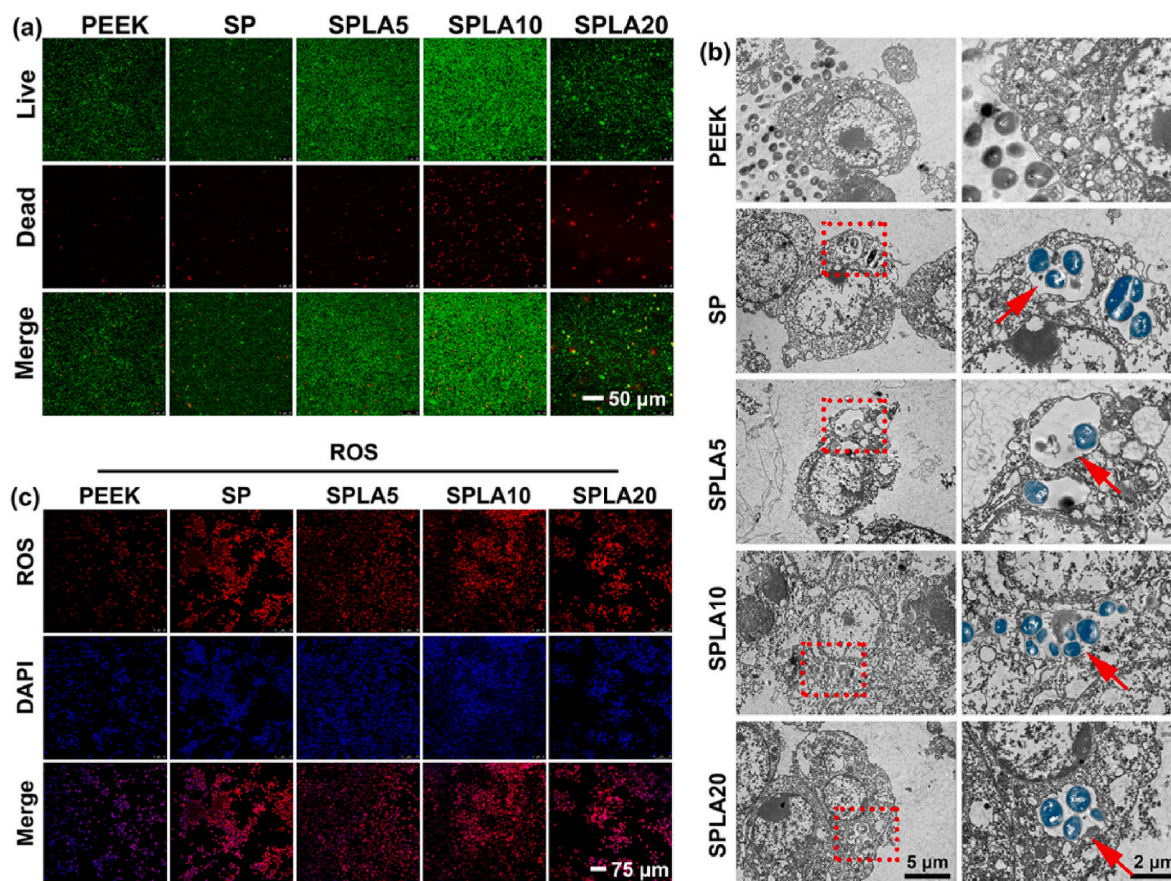
**Fig. 3. Anti-*S. aureus* activity by macrophages stimulated with samples.** (a) Live/dead bacteria staining images of bacteria co-cultured with macrophages on the samples; (b) TEM images of intracellular bacteria in macrophages after stimulated by samples (the intracellular bacteria are marked by red arrows); (c) Intracellular ROS staining images of macrophages cultured on samples for 4 days.

expression of rBMSCs cultured on SPLA10 surface is also the highest (Fig. 4e and f). In summary, L-Arg could enhance Col-III and Col-II expression in L929 and rBMSCs respectively, which is beneficial for soft and hard tissue regeneration.

### 2.5. In vivo soft tissue sealing

The soft tissue sealing model was used to study the effect of samples on infected percutaneous tissue healing. Giemsa staining was used to label bacteria *in vivo*, and the results are shown in Fig. 5a and b, and Fig. S10. After implantation for 1 day, there are many bacteria dispersed in the tissue around PEEK, however, the bacteria in the tissue around the samples with sulfonation is decreased. SPLA10 shows the fewest bacteria in the tissue, and attenuated antibacterial proportion appears with decreased L-Arg released content. Notably, the dispersity of bacteria in PEEK is higher than that in the other four groups, which indicates that a spreading infection occurs around PEEK. After implantation for 4 days, the number of bacteria in tissues of the groups loading with L-Arg is remarkably reduced than 1 day. SPLA10 remains the superior antibacterial property than the other four groups.

To determine the mechanism of L-Arg loading samples in bacteria elimination, RNA-Seq was used to test the genes expressions in tissue after implantation with PEEK and SPLA10 for 4 days, and the results are shown in Fig. 5c–e. Heat map and volcano plot of the different genes expressions show that 69 genes are significantly changed (q-value <0.05 and | $\log_2$FC |>1). There are 24 downregulated genes and 45 upregulated genes (Fig. S11a and b). Circos graph of KEGG enrichment shows that four types of pathways are enriched, including organismal systems, metabolism, human diseases, and environmental information processing

(Fig. S12a). The bubble diagram of KEGG enriched top 20 pathways of upregulated genes shows that phagosome may be tightly related to the bacteria elimination of SPLA10 (Fig. 5c). The chord chart of KEGG enriched top 10 pathways exhibits that complement and coagulation cascades pathway is related to bacteria elimination. Further, the complement and coagulation cascades pathway are significantly higher expressed in the SPLA10 group (Fig. S12b). Gene set enrichment analysis (GSEA) based on the RNA-Seq data was used to further analyzed pivotal pathway and gene. The results show that genes in phagosome are significantly enriched after implantation with SPLA10 (Fig. 5d). The heat map of top 20 genes expressions in leading-edge subset shows that C3 may play pivotal role in regulation of phagocytizing bacteria (Fig. 5e). In summary, RNA-Seq data analysis shows that SPLA10 may improve the cell phagosome through C3 mediated complement and receptor activation. To verify this hypothesis, C3 expression of tissue around the samples was detected by Western blot, and the results are shown in Fig. 5f and g. After implantation for 1 day, C3 protein expression in SPLA10 group is significantly higher than that in PEEK group. While, the α chain and α chain fragment of iC3b are not upregulated. After implantation for 4 days, there is not any significance between PEEK and SPLA10 group. Conversely, the α chain and α chain fragment of iC3b in SPLA10 group are remarkably upregulated than PEEK group, especially for α chain fragment of iC3b.

To clear the pathways transformation from infection phase to repair phase, we analyzed differential genes expression of SPLA10 after implantation for 4 days and 14 days. There are five types of pathways are enriched, including human diseases, organismal systems, metabolism, environmental information processing, and cellular processes (Fig. 6a). The bubble diagram of KEGG enrichment shows that the upregulated
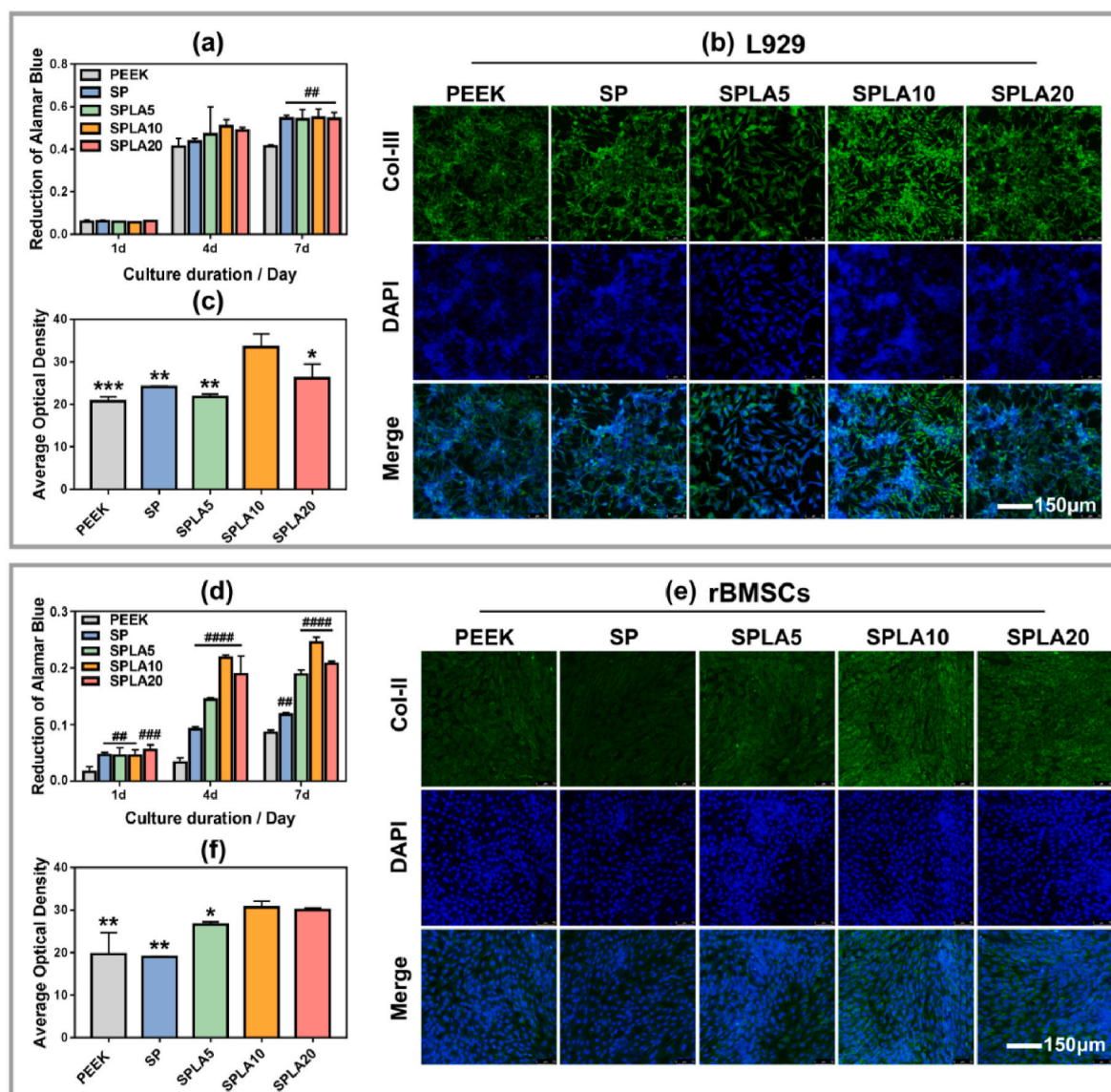
**Fig. 4. Collagen secretion of cells.** (a) Proliferation of L929 cultured on the surface of samples (n = 4); (b) Representative immunofluorescent staining images of L929 co-cultured with macrophages on the surface of samples; (c) The quantitative average of optical density of the immunofluorescent staining images of L929 co-cultured with macrophages on the surface of samples (n = 3); (d) Proliferation of rBMSCs cultured on the surface of samples (n = 3); (e) Representative immunofluorescent staining images of rBMSCs co-cultured with macrophages on the surface of samples; (f) The quantitative average of optical density of the immunofluorescent staining images of rBMSCs co-cultured with macrophages on the surface of samples (n = 3); Data are expressed by mean with SD. Statistical significance was calculated by one-way ANOVA analysis, two-way ANOVA analysis and Tukey's multiple comparison tests. ##$p < 0.01$ and ####$p < 0.0001$, compared with PEEK in a and d. *$p < 0.05$, **$p < 0.01$ and ***$p < 0.001$, compared with SPLA10 in c and f.

genes in SPLA10 group after implantation for 14 days are enriched to the tissue repair related pathways, including cell adhesion molecules, melanogenesis, and axon guidance and so on (Fig. 6b). The down-regulated genes in SPLA10 group after implantation for 14 days are enriched to some infection related pathways, including phagosome, Toll-like receptor signaling pathway, and chemokine signaling pathway and so on (Fig. 6c), which indicates that the infection is diminished after 14 days implantation with SPLA10 compared to 4 days implantation.

As the results of infection control, macrophages tend to polarize to M2 phenotype. The immunofluorescence staining shows that Arg-1 expression is obviously higher in SPLA10 group than the other four groups (Fig. 6d). The quantitative results show that compared with PEEK and SP, there are less M1 and more M2 on the surface of samples loading with L-Arg. Among them, SPLA10 group has the highest M2/M1 ratio (Fig. S13). The cutaneous tag around SPLA10 does not prolong to the deep of the samples, which is beneficial for impeding bacteria

residence (Fig. 6e). Masson staining shows that more blue marked collagen fiber could be observed in SPLA10 group (Fig. 6f and Fig. S14a). The immunohistochemical staining of Col-III was applied for further determination of collagen secretion in tissue around the samples. The positive area of Col-III in SPLA10 and SPLA20 is more than that in PEEK, SP, and SPLA5 groups (Fig. 6g and Fig. S14b). In addition, Fig. 6h shows that there is more CD31 labeled positive area around the samples loading with L-Arg compared with PEEK and SP, especially in SPLA10 (Fig. S15). The above results disclose that SPLA10 could improve infected soft tissue sealing through polarizing macrophage to M2 and promoting Col-III secretion and angiogenesis.

### 2.6. In vivo bone regeneration

Except for superior soft tissue sealing, the success of percutaneous implantation requires superior bone regeneration. Herewith, the
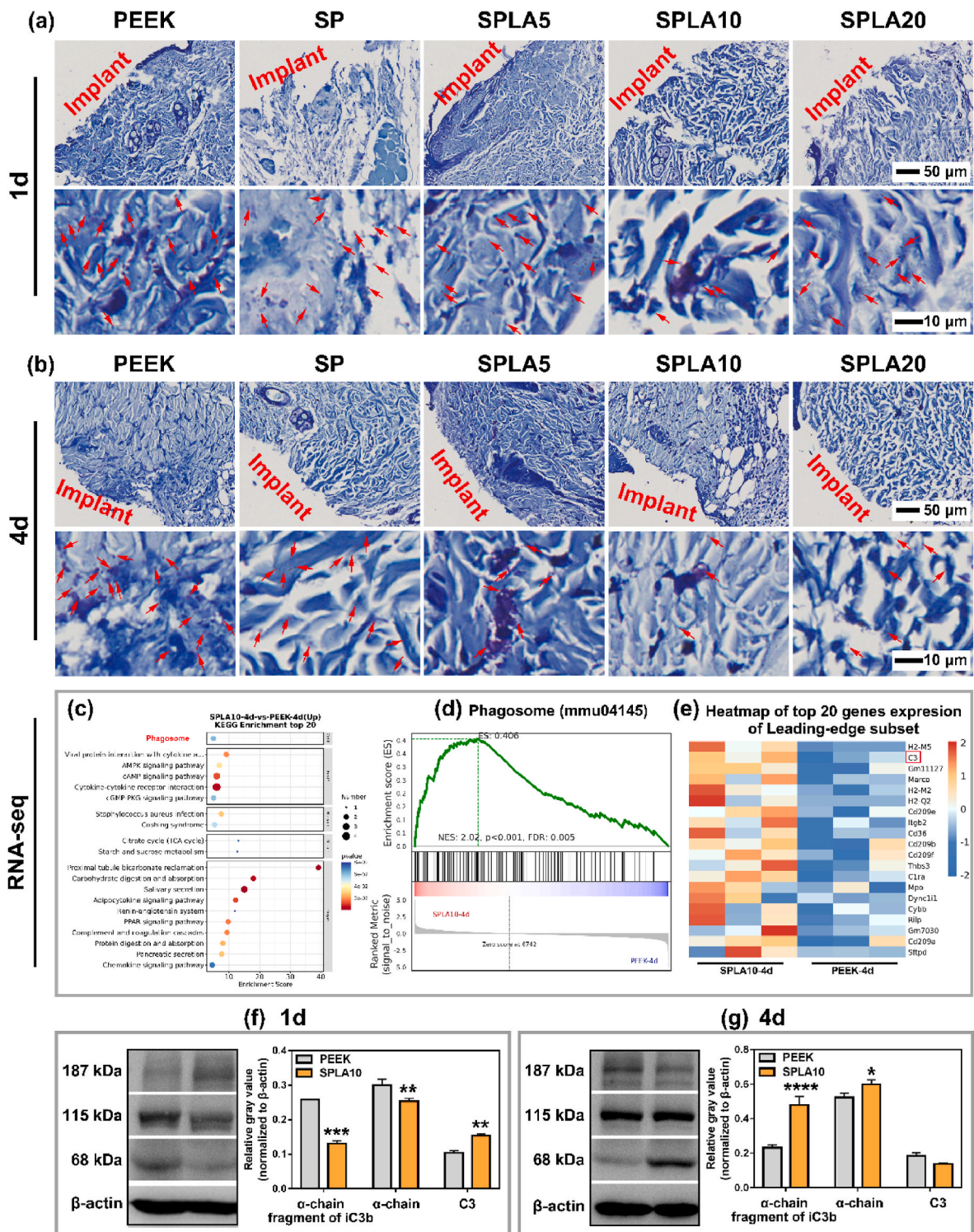
**Fig. 5. Bacterial response *in vivo*.** (a) Representative images of Giemsa staining of skin around the samples post implantation for 1 day with lower and higher magnification; (b) Representative images of Giemsa staining of skin around the samples post implantation for 4 days with lower and higher magnification (The red arrows mark the bacteria stained with dark purple); (c) Bubble diagram of KEGG enriched top 20 pathways of upregulated genes; (d) Enrichment score of the phagosome and (e) heat map of top 20 genes in leading-edge subset expressed in SPLA10 versus PEEK control group analyzed by GSEA based on the RNA-seq datasets; (f) α-chain fragment of iC3b, α-chain and C3 protein expression in skin around samples post implantation for 1 day analyzed by Western Blot (n = 3); (g) α-chain fragment of iC3b, α-chain and C3 protein expression in the skin around samples post implantation for 4 days analyzed by Western Blot (n = 3). Data are expressed by mean with SD. Statistical significance was calculated by two-way ANOVA analysis and Tukey's multiple comparison tests. *p < 0.05, **p < 0.01, ***p < 0.001, ****p < 0.0001, compared with PEEK in f and g.
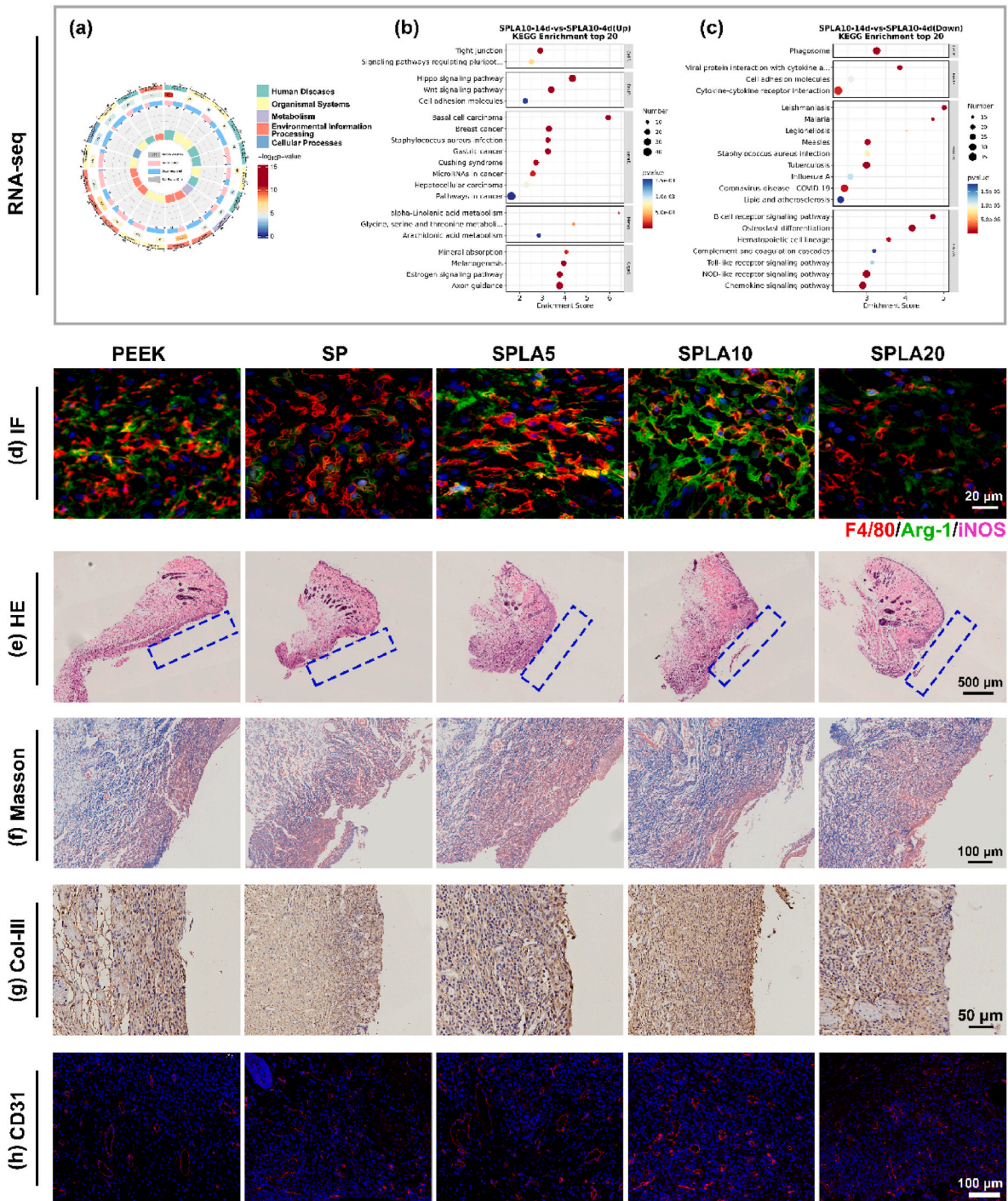
**Fig. 6. Soft tissue healing.** (a) Circos graph of KEGG enrichment; (b) Bubble diagram of KEGG enriched top 20 pathways of upregulated genes; (c) Bubble diagram of KEGG enriched top 20 pathways of downregulated genes; (d) Representative immunofluorescent staining images of macrophages in skin tissue implanted with samples for 14 days (F4/80 labeled macrophages with red, iNOS labeled M1 with pink, Arg-1 labeled M2 with green); (e) Representative HE staining images of skin tissue implanted with samples for 14 days (the implants are marked by dotted box); (f) Representative Masson staining images of skin tissue implanted with samples for 14 days; (g) Representative Col-III staining images of skin tissue implanted with samples for 14 days; (h) Representative CD31 staining images of skin tissue implanted with samples for 14 days.

samples were inserted into the infected bone defect model to detect their effect on repair. After implantation for 1 month, the bone femur with sample was scanned by micro-CT, and the results are shown in Fig. 7. The coronal and transaxial two dimensional reconstructed micro-CT images of the bone implanted with samples for 1 month show that there is more bone tissue around SPLA10 than the other four groups (Fig. 7a). Three dimensional reconstructed micro-CT images of the

newly formed bone implanted with samples for 1 month also verified it and the bone is denser in SPLA10 group (Fig. 7b). The rate of bone volume to tissue volume (BV/TV) of SPLA10 group is highest, followed by SPLA20, SPLA5, SP and PEEK (Fig. 7c).

To further gain knowledge of the quality of newly formed bone, the bone parameters, including trabecular number (Tb.N), trabecular thickness (Tb.Th), trabecular pattern factor (Tb.Pf), structure model
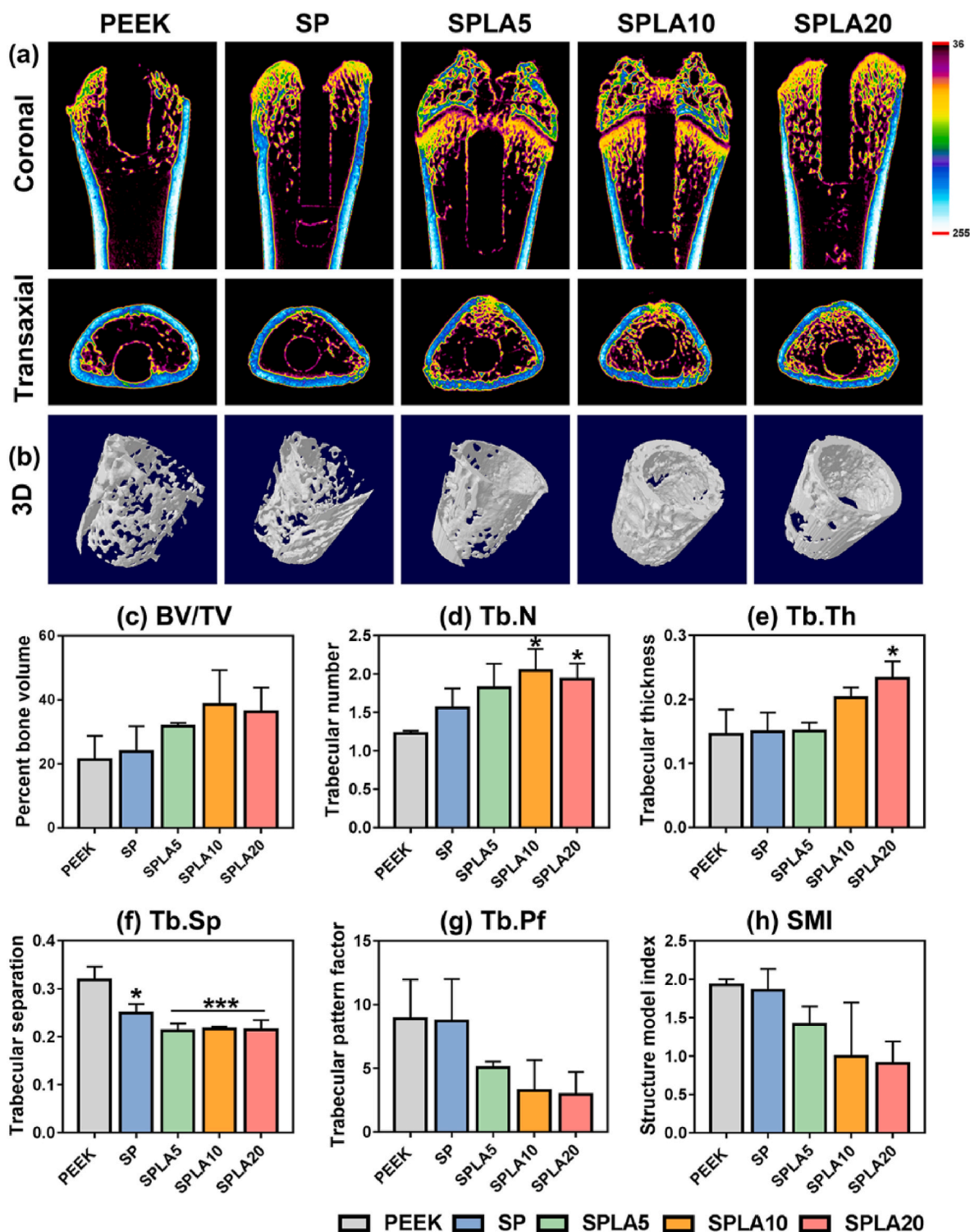
**Fig. 7. Bone regeneration of the samples.** (a) Two dimensional reconstructed micro-CT images of the bone implanted with samples for 1 month; (b) Three dimensional reconstructed micro-CT images of the newly formed bone implanted with samples for 1 month; (c) Quantitative bone volume/tissue volume, (d) Trabecular number, (e) Trabecular thickness, (f) Trabecular spacing, (g) Trabecular pattern factor and (h) Structure model index. Data are presented by mean with SD, n = 3. Statistical significance was calculated by one-way ANOVA analysis. *$p < 0.05$, ***$p < 0.001$, compared with PEEK in c-h.

index (SMI), and trabecular spacing (Tb.Sp), are analyzed (Fig. 7d–h). The quantitative Tb.N shows that there are more intersection of bone and non-bone tissue in SPLA10 and SPLA20 groups (Fig. 7d). The thickness of trabecula in these two groups are also higher than PEEK, SP and SPLA5 (Fig. 7e). The mean width of the medullary space between bone trabecula of L-Arg loading sulfonated samples are remarkably

lower than PEEK (Fig. 7f). Tb.N, Tb.Th and Tb.Sp analysis show that SPLA10 can improve the trabecula structure. The morphology of newly formed trabecula is analyzed by Tb.Pf and SMI (Fig. 7 g and h). Tb.Pf is the parameter to show concavity of trabecula, its increase indicates that the trabecular transforms plate to rod in osteoporosis bone. SPLA10 could decrease the Tb.Pf compared to PEEK, which indicates that L-Arg

could improve rod trabecula formation. Also, this phenomenon is veri- fied by SMI. The rate of plate trabecula and rod trabecula are closer to 0 in SPLA10 and SPLA20 groups, while closer to 3 in PEEK and SP groups. It can be concluded that SPLA10 could improve bone strength and bone mass.

Histological analysis was applied to further analyze the newly formed bone. Fig. 8a shows the HE staining images of the adjacent tissue of samples. More bone tissue is observed around SPLA10, while there is little bone tissue around PEEK. Quantitative analysis shows that the bone area SPLA10 is significantly more than the other groups (Fig. 8b). The high magnification of HE staining shows that there are some neu- trophils around the samples in PEEK, SP and SPLA5 (green arrows

marked), while the neutrophils are hardly observed in SPLA10 and SPLA20. Notably, the vessels can be observed around SPLA10 (blue arrows marked). Furthermore, immunohistochemical staining for la- beling neutrophils (labeled by LY6G) and immunofluorescence staining of macrophage phenotype (CD68/iNOS/CD206) were performed to observe the inflammatory response in bone tissues. The results show that SPLA10 and SPLA20 groups could significantly reduce neutrophil infil- tration compared with the other three groups (Fig. S16), and the groups loading with L-Arg have higher M2/M1 ratio than PEEK and SP groups with the increased L-Arg release (Fig. S17). In addition, immunohisto- chemical staining shows that Col-II expression in SPLA10 is slightly higher than that in SPLA20, which is consistent with the Col-II
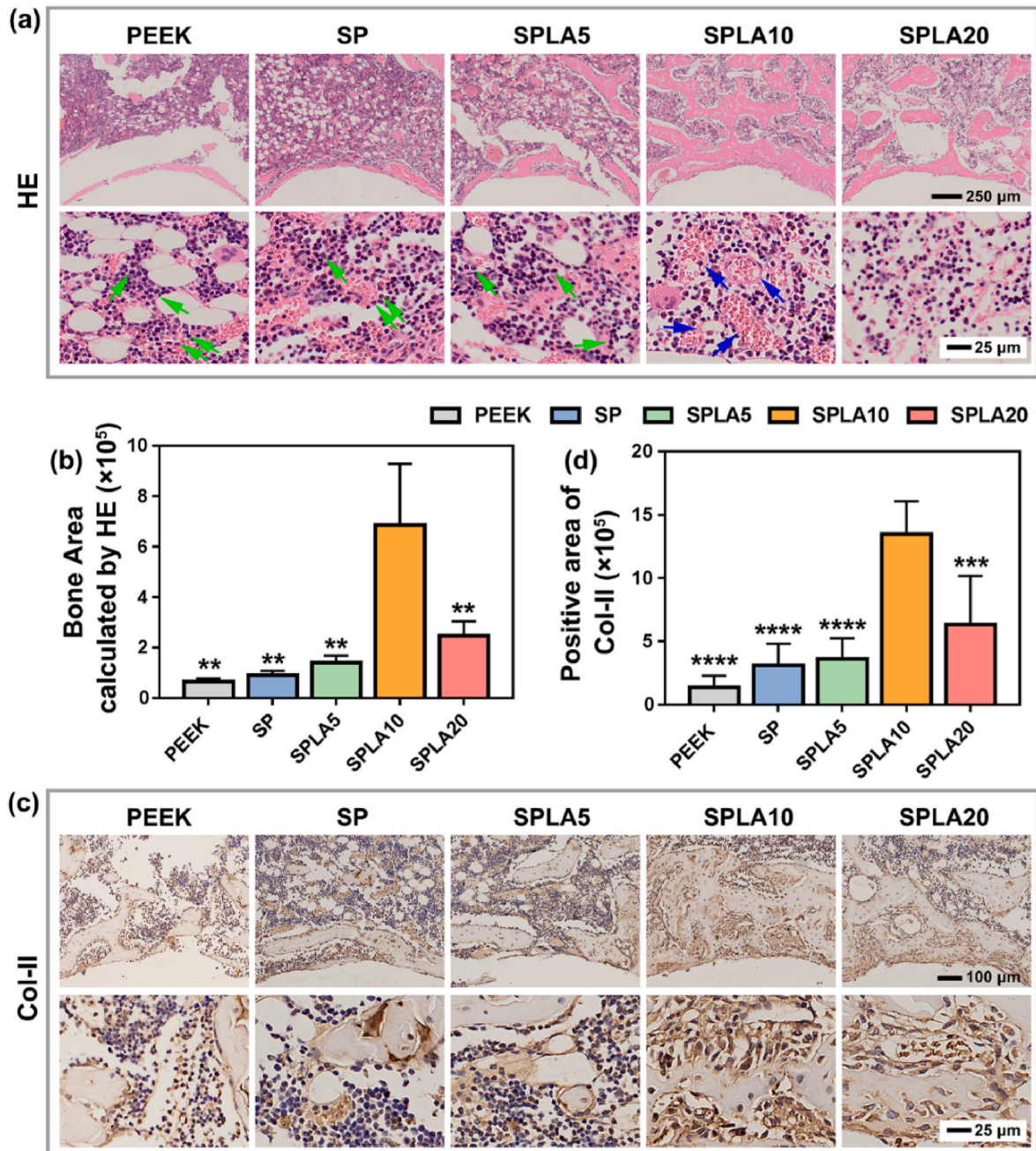


**Fig. 8. Histological analysis of the tissue around samples.** (a) Representative HE staining images of tissue around the samples post implantation for 1 month (the green arrows mark the neutrophil in tissue around samples and the blue arrows mark the newly formed vessels in the tissue around samples). (b) Quantitative bone area calculated by HE (n = 3); (c) Represent Col-II staining images of bone tissue around the samples post implantation for 1 month; (d) Quantitative positive area of Col-II (n = 4). Data are presented by mean with SD. Statistical significance was calculated by one-way ANOVA analysis. **p < 0.01, ***p < 0.001, ****p < 0.0001, compared with SPLA10 in b and d.

expression *in vitro* (Fig. 8c and d). There is less positive Col-II area in PEEK, SP and SPLA5 than SPLA10 and SPLA20. In summary, SPLA10 could improve new bone formation, angiogenesis, and Col-II expression.

## 3. Discussions

Traditional materials design often solves problems in an object-oriented way. Structure, metal ions, drugs and peptides that possess antibacterial abilities are usually used to construct materials for sterilizing bacteria. The materials that can regulate endothelial cells and fibroblasts are constructed to deal with inferior vessel reconstruction. The structure and chemical molecule that can regulate BMSCs, osteoblast and osteoclast are designed onto the substrate material to improve hard tissue regeneration. It can meet several demands through combining the above strategies. However, it is hard to construct a simple material that can cope with the comprehensive issue of percutaneous implants due to its special environment, including infection, soft tissue sealing and hard tissue regeneration. Different from the traditional strategies of materials improving the specific cell function, macrophage-related immunomodulation material plays a pivotal role in tissue repair through secreting cytokines that act on a variety of cells. Therefore, it is a new idea to obtain materials with adaptive sequential macrophage polarization through metabolic reprogramming. Our previous work fabricated the polypyrrole modified surface on PEEK, which could sequentially regulate macrophage phenotype through controlling NIR stimuli [5]. In this work, L-Arg was loaded onto the porous sulfonated PEEK surface to acquire adaptively sequential macrophage phenotype regulation. We found that L-Arg loading PEEK could be catalyzed to different metabolites to paly role in macrophage polarization, and thus kill bacteria at infection stage and promote soft and hard tissue repair after clearing bacteria.

Literatures have been disclose that it is important to regulate the L-Arg content released from material [14]. Li et al. controlled the release of Arg carbon dots in hydrogels to produce excess reactive oxygen species (ROS) to kill bacteria while promote M2 polarization to improve the bone formation through up-regulating the expression of antioxidant enzymes [28]. Control of L-Arg release is also the key point to successfully realize the sequential macrophage polarization through reprogramming metabolic of macrophage under different environments in this work. Three group samples with different L-Arg content are prepared in this work. With the increase of L-Arg loading content, the less sulfonic acid group is exposed, resulting in the increase of Zeta potential. The amino end of L-Arg is oriented towards the sulfonyl group by electrostatic action, while the carboxyl end is exposed, resulting in a decrease of Zeta potential. As comprehensive outcomes of above two reasons, SPLA5 exhibits a higher Zeta potential than SP and SPLA10. While SPLA20 shows a lower Zeta potential than SP, SPLA5, and SPLA10. The release content of L-Arg is affected by surface morphology and loading content. As the lowest L-Arg loading content of SPLA5 and high L-Arg agglomeration of SPLA20, SPLA10 exhibits highest L-Arg release.

At the infection stage, macrophages choose efficient glycolysis to rapidly obtain adenosine triphosphate (ATP) and interrupt the TCA cycle to obtain bactericidal substances, play the role of clearing and killing harmful microorganisms, and maintain the continuous polarization of M1 macrophages. Pentose phosphate pathway (PPP) promotes fatty acid synthesis (FAS), produces a large amount of reducing coenzyme II (NADPH), promotes the expression of NADPH oxidase (NOX) and iNOS, and induces ROS/NO to kill pathogenic microorganisms. In addition, proline hydroxylase (PHD) is inhibited and HIF-1α stability is improved. Since iNOS is the target of HIF-1α, the positive feedback loop further amplifies the induction of HIF-1α through NO-mediated PHD inhibition, which can maintain the continuous activation of M1 macrophages [31]. Two interruptions in the TCA cycle lead to the accumulation of citric acid and succinic acid, which play a role in sterilization and promoting M1 polarization [24]. First, the accumulation of citrate leads to an increase of the synthesis of FA and itaconate,

which directly plays a bactericidal role. Meanwhile, ROS and NO can be produced by NADPH to participate in bactericidal action. Secondly, the second rupture of TCA results in the accumulation of succinic acid, which promotes the activation of HIF-1α and the expression of IL-1β. The shunt of aramidine succinate also helps replenishing fumarate in the TCA cycle and killing microorganisms by producing NO. In addition, the oxidation of succinic acid inhibits the activity of PHD and stabilizes the expression of HIF-1α, thus promoting the activation of M1 macrophages. L-Arg is the substrate of iNOS that participate in anti-infection through producing NO [16,19]. Loading L-Arg on sulfonated PEEK achieves to promote M1 polarization and high iNOS expression, thus producing more NO to kill bacteria.

After infection is controlled, the metabolic pathway of macrophages changes from glycolysis and interrupted TCA cycle to complete TCA cycle and oxidative phosphorylation, thus promoting the transformation of macrophages from M1 type to M2 type, and playing the role in promoting tissue repair. Complete TCA cycle inhibits M1 macrophage polarization. On the one hand, α-ketoglutaric acid, an important metabolite of the TCA cycle, can inhibit M1 macrophage activation by inhibiting HIF-1α and HIF-1β related metabolic metabolic pathways. On the other hand, the complete TCA cycle can consume the accumulated succinic acid and citric acid in the pro-inflammatory stage, thus weakening the relevant pro-inflammatory level caused by ROS and reducing the polarization of M1 [32]. Oxidative phosphorylation promotes the activation of M2 macrophages by supplying fatty acid oxidation and TCA. Mitochondria uses NADPH and FADH2, the main products of TCA, to supply electrons to the electron transport chain (ETC), support the process of oxidative phosphorylation, and obtain high efficiency ATP. At the same time, mitochondria also obtain the oxidation products of nutrients, and produce repair-related factors through toxicological excitation to promote tissue remodeling and wound healing [33]. Under this condition, sulfonated PEEK loading with L-Arg can stimulate M2 polarization and high Arg-1 expression to promote the metabolism of ornithine, which finally increases the collagen secretion in the tissues.

Complement is family of proteins and proteolytic fragments possessing heat-resistance and enzyme-activation, and could mediate immune response and inflammation in serum and interstitial fluid. It contains more than 30 kinds of soluble proteins and membrane binding proteins, which play pivotal role in effector molecules recruitment and labeling bacteria for further target and destruction [34]. C3 composes by α and β peptide chain, which would be hydrolyzed to α fragment (C3a) and C3b. C3a has a chemotactic effect that causes phagocytes to move in a directional manner to promote phagocytosis. C3b is then further processed by factors H and I to produce iC3b, which is one of the main opsonins. C3b and iC3b could combine with the complement receptor of macrophage surface to promote phagocytosis as well. Especially, iC3b exhibits higher affinity to complement receptors 3 and 4 [35]. At 1 day, more C3 is accumulated and hydrolyzed to fragments for labeling bacteria in SPLA10 group, which is helpful for immune cells recognition. However, the produced C3 fragments is consumed for bacteria elimination, so α-chain fragment of iC3b and α-chain in SPLA10 group exhibit a slight decrease than PEEK group. At 4 days, most of the bacteria are eliminated by immune cells. Therefore, C3 accumulation is decreased and α-chain fragment of iC3b and α-chain in SPLA10 group are accumulated.

Benefiting from the multi-functions of L-Arg, the samples could obtain both antibacterial abilities and tissue repair, including soft tissue healing and hard tissue regeneration (Fig. 9). Under the infection conditions, L-Arg is catalyzed by iNOS thus producing NO and ROS to play the role in sterilization. When the conditions transform to tissue repair, L-Arg is catalyzed by Arg-1 thus producing ornithine to enhance cell proliferation and collagen secretion. Notably, the macrophages would not polarize to M1 or M2 with the increased L-Arg content immoderately, which indicates that L-Arg loading samples could regulate their phenotypes adaptively. The cues that related to this phenomenon may be account to the feedback regulation.
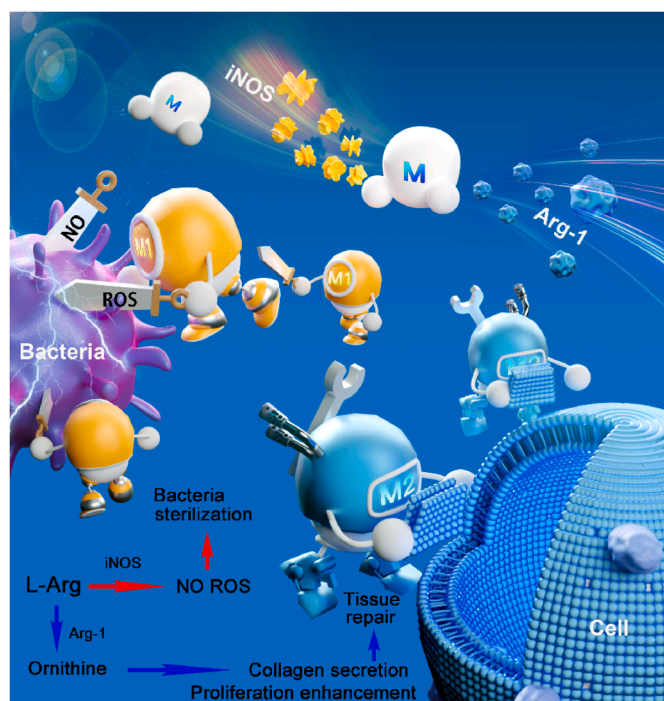
**Fig. 9. The schematic illustration of the effect of L-Arg loading PEEK on both antibacterial abilities and tissue repair, including soft tissue healing and hard tissue regeneration, by macrophage orchestration *via* metabolic reprogramming.** Under infection condition, macrophage polarizes to M1 and L-Arg is catalyzed to NO and ROS by iNOS, which play the role in sterilization. Under the tissue repair condition, macrophage will polarize to M2 and L-Arg is catalyzed to ornithine by Arg-1, which promotes the proliferation and collagen secretion of cells.

## 4. Conclusions

The as prepared L-Arg loading sulfonated PEEK in this work could sequentially polarize macrophage to M1 and M2 through metabolic reprogramming. In detail, L-Arg is catalyzed by iNOS to NO, which maintains M1 polarization and participates in bacteria sterilization under infected condition induced by LPS and bacteria; L-Arg is catalyzed by Arg-1 to ornithine, which promotes cell proliferation, Col-III secretion of L929, and Col-II of rBMSCs. Also, macrophage tends to polarize to M2 under IL-4 stimulation. The results *in vivo* show that L-Arg loading sulfonated PEEK could promote infected soft tissue sealing through sterilizing bacteria, enhancing collagen secretion. Besides, the samples loading with L-Arg could accelerate new bone formation and vessel reconstruction. Based on the above advantages of L-Arg loading samples, it can be a good alternative strategy for percutaneous implantation materials design.

## 5. Experimental methods

### 5.1. Sample preparation

Medical grade PEEK slices ($\Phi$ 10 mm $\times$ 1 mm and 20 mm $\times$ 10 mm $\times$ 1 mm) and rods ($\Phi$ 2 mm $\times$ 18 mm and $\Phi$ 1.8 mm $\times$ 6 mm) were ultrasonically washed with ethanol and ddH$_2$O subsequently. They were dried and named PEEK for use. All samples were sulfonated by immersing in 98 % concentrated sulfuric acid with magnetically stirring at room temperature for 10 min to obtain a uniform 3D porous structure. Then the samples were soaked in ddH$_2$O for 10 min to remove residual concentrated sulfuric acid. Next, the samples were treated at 120 °C for 5 h to remove excess sulfur, washed with ddH$_2$O twice, and dried at room temperature. After that, all samples were radiated with ultraviolet

rays overnight before biological experiments. The sulfonated PEEK samples were named SP. SP samples were immersed into different concentrations of L-Arg solution (5 mM, 10 mM, and 20 mM) and oscillated in 60 r/min at 37 °C for 24 h, then washed with sterilized water and dried naturally on a super clean table. These samples were named SPLA5, SPLA10, and SPLA20, respectively. All samples were placed in a sterile environment for further experiments. Among them, the disc samples were used for material characterization and *in vitro* biological experiment, the rectangular samples were used for surface Zeta potential test, the rod samples ($\Phi$ 2 mm $\times$ 18 mm) were used for percutaneous implantation model, and the rod samples ($\Phi$ 1.8 mm $\times$ 6 mm) were used for rat osteomyelitis model.

### 5.2. Surface morphology and composition characterization

The surface morphologies of PEEK, SP, SPLA5, SPLA10, and SPLA20 samples were observed by field emission scanning electron microscopy (FEI-SEM, Magellan 400, USA). An infrared spectrometer (Tensor 27, Bruker, Germany) was used to detect the surface groups of the samples. XPS (Thermo Scientific K-Alpha) was used to detect the composition and content of elements on the samples surface (three replicates).

### 5.3. Surface contact angle test

The surface wettability of PEEK, SP, SPLA5, SPLA10, and SPLA20 samples was evaluated using a static water contact angle measuring instrument (SL200B, Solon, Shanghai). At room temperature, 2 µL of ultra-pure water was dropped on samples. After stabilizing, take pictures with the camera and read the contact angle value through the computer software.

### 5.4. Surface zeta potential test

The curve of surface zeta potential of PEEK, SP, SPLA5, SPLA10, and SPLA20 samples as a function of the pH of KCl electrolyte solution was detected by the Surpass electrokinetic analyzer (Anton Parr, Austria), as described in the previous work [7].

### 5.5. L-Arg release

SPLA5, SPLA10, and SPLA20 samples were immersed in 1 mL of ddH$_2$O, and then placed in a 37 °C incubator. The soaking solution of 1, 4, 7, 14, 21, and 28d were collected. The L-Arg concentration was determined by Arginine assay kit (Biovision, K384-100, USA), and the operation was according to the protocol.

### 5.6. Cell experiments

**Cell culture:** Mouse-derived mononuclear macrophage leukemia cells (RAW264.7, Cell Bank, Chinese Academy of Sciences, China) were chose for studies *in vitro* [36–38]. The cells were seeded in cell culture flasks and cultured in high-glucose Dulbecco's modified Eagle's medium (DMEM, Gibco, USA) containing 1 % penicillin and streptomycin (Gibco, USA) and 10 % fetal bovine serum (FBS, Gibco, USA), maintained at 37 °C in a humidified atmosphere with 5 % CO$_2$. L929 and rBMSCs were seeded in cell culture flasks cultured with α-minimum essential medium (α-MEM, Gibco, USA) containing 1 % penicillin and streptomycin (Gibco, USA) and 10 % FBS (Gibco, USA), maintained at 37 °C in a humidified atmosphere with 5 % CO$_2$. The cells were passaged every 3 days at a ratio of 1: 3.

**In vitro co-culture:** The L929 cells or rBMSCs were inoculated at a density of 2 $\times$ 10$^4$ cells/well on cell crawling slides for 4 days. RAW264.7 cells were inoculated on the samples surface at a density of 5 $\times$ 10$^4$ cells/samples stimulated with IL-4 (10 ng/mL) for 1 day. Then the samples seeded with RAW264.7 and the cell crawling slides seeded with L929 cells or rBMSCs were placed together in a 6-well plate with

continuous 10 ng/mL IL-4 stimulation and incubated for another 3 days.

***Cell proliferation:*** L929 cells or rBMSCs were seeded on different samples with a density of $2 \times 10^4$ per well and cultured in 24-well plates for 1 day, 4 days, and 7 days. Cell proliferation was evaluated by alamarBlue™ assay (Thermo Fisher Scientific, USA). At every point in time, each well was added 500 μL of fresh full culture medium with 10 % alamarBlue™ and incubated for another 3 h in dark. Then, 100 μL of the above solution was taken out and added to a 96-well plate. The absorbance at 570 nm and 600 nm was detected by a microplate reader (Multiskan GO, Thermo Fisher Scientific, USA) to evaluate the cell proliferation.

***Immunofluorescence staining:*** By antigen-antibody binding, marker proteins for distinct macrophage phenotypes were fluorescently labeled, and the surface fluorescence density was tested to determine the macrophage phenotype of diverse samples. RAW264.7 cells were seeded on the cell crawling slides with samples in upper chamber at a density of $5 \times 10^4$ per well in a 24-well plate. The cells were stimulated with LPS (10 ng/mL) and IL-4 (10 ng/mL) for 4 days. The cells were fixed with 4 % paraformaldehyde at 4 °C overnight after being washed by PBS. The cells were then permeabilized with 0.1 % Triton X-100 for 5 min and blocked with 1 wt% BSA for 2 h, and each step was followed by twice PBS washes to remove residual reagents. Then, cells were incubated with specific primary antibodies, goat polyclonal anti-CCR7 antibody (Novus, NB100–712SS, 1: 200), rabbit polyclonal anti-iNOS antibody (Abcam, ab3523, 1: 50), rabbit monoclonal anti-CD206 antibody (Cell Signaling Technology, 24595, 1: 200), mouse monoclonal anti-Arg-1 antibody (Abcam, ab239731, 1: 50), rabbit monoclonal anti-Col-III antibody (Abcam, ab184993, 1: 50) and rabbit polyclonal anti-Col-II antibody (Abcam, ab34712, 1: 50) at 4 °C overnight. Afterward, cells were incubated with secondary antibodies, donkey anti-goat IgG H&L Alexa Fluor 594 (Abcam, ab150132, 1: 200), donkey anti-rabbit IgG H&L Alexa Fluor 488 (Abcam, ab150073, 1: 200) and goat anti-mouse IgG H&L Alexa Fluor 594 (Abcam, ab150116, 1: 200) for 2 h in the dark. After washing with PBS, 4',6-diamidino-2-phenylindole (DAPI) was used to stain the nuclei in the dark at room temperature for 10 min. A confocal laser scanning microscope (TCS SP8 SR, Leica, Germany) was used for observation, which was then analyzed with ImagePro software.

***Macrophage metabolites determination:*** RAW264.7 cells were seeded on the surface of samples with a density of $5 \times 10^4$ per well. The cells were stimulated with LPS (10 ng/mL) and IL-4 (10 ng/mL) respectively and cultured at 37 °C for 4 days. Subsequently, the culture solution was collected and used to test the concentration of ornithine and nitric oxide by nitric oxide assay kit (Beyotime, S0023, China) and ornithine Assay Kit (Fluorometric, Biovision, K939-100, USA) respectively according to the manufacturers' protocols.

***Intracellular reactive oxygen species (ROS):*** RAW264.7 cells were seeded on the cell crawling slides with samples in upper chamber at a density of $5 \times 10^4$ per well in a 24-well plate. The cells were stimulated with LPS (10 ng/mL) and incubated at 37 °C for 1 day and 4 days. After two washes with PBS, 2′,7′-dichlorodihydrofluorescein diacetate (DCFH-DA) (Beyotime, China) diluted with serum-free culture medium was applied to the cell surface and incubated at 37 °C for 20 min in dark. After washing off the residual DCFH-DA with PBS, the nuclei were stained with DAPI for 10 min at room temperature and protected from light. Confocal laser scanning microscope (TCS SP8 SR, Leica, Germany) was used for observation. The test was performed on day 1 and day 4 of RAW264.7 culture. ROS in macrophages was labeled with DCFH-DA probes. Then macrophages were collected by enzyme and the fluorescence intensity of ROS was tested. The macrophage quantity was tested using alamar blue™ at each time point. The relative ROS content was normalized by cell quantity.

## 5.7. Bacteria experiments

***Co-culture condition of bacteria:*** Gram-positive Staphylococcus aureus (*S. aureus*, ATCC 25923) was used to evaluate the effect of macrophage cultured on samples on bacteria. *S. aureus* was cultured with trypsin soybean broth (TSB, Aladdin), and the bacteria at logarithmic growth stage were selected for experiment.

Macrophages were inoculated on the surface of samples at a density of $1 \times 10^5$ cells per well and cultured for 4 days. The culture medium did not contain any antibiotics. Then the samples cultured with macrophages and 720 μL of corresponding medium were transferred to a new 24-well plate, added with 80 μL *S. aureus* ($1 \times 10^8$ CFU/mL), and incubated in an incubator at 37 °C for another 3 h.

***Live/dead staining of bacteria:*** After the bacteria were co-cultured with macrophages stimulated by samples, the culture solution was collected, and the surface macrophages were digested with 0.05 % trypsin to obtain a cell-bacterial mixture. The above mixed solution was collected into 1.5 mL EP tube, and bacteria and cells were separated by centrifugation at $400 \times g$ for 5 min. Then the supernatant was collected and continued centrifugation at $12,000 \times g$ for 1 min to obtain bacterial clumps. The live/dead bacteria were stained using a bacterial viability assay kit (L13152, Thermo Fisher Scientific Inc., USA). After cleaning twice through PBS to remove excess fluorescent dye, 50 μL PBS was added to each group of tubes for re-suspension bacteria. The confocal laser microscopy (TCS SP8 SR, Leica, Germany) was used to observe bacterial activity.

***Bacterial activity:*** The bacteria, supernate, and samples were collected into 1.5 mL EP tube, and the bacteria-cell mixed solution was obtained by shaking. The mixed solution was centrifuged at $400 \times g$ for 5 min. Then the supernatant was transferred to a new centrifuge tube, centrifuged at $12,000 \times g$ for 1 min. The supernatant was removed to obtain bacterial clumps. 500 μL of normal saline containing 10 % alamarBlue™ (Thermo Fisher Scientific Inc., USA) was added to each tube and incubated at 37 °C for 2 h. The above solution of 100 μL was absorbed to test the bacterial activity.

***Bacterial morphology:*** The mixture of macrophages and bacteria was collected in 1.5 EP tubes and centrifuged at $12,000 \times g$ for 1 min to collect cell-bacterial clumps. After washing twice with PBS, 1 mL of 2.5 vol % glutaraldehyde solution was added to fix cell - bacterial clumps. After centrifuging again, cell - bacterial clumps were pre-embedded with agarose and fixed with PBS solution containing 1 % OsO₄ (Ted Pella Inc) for 2 h 30 %–50 % - 70 %–95 % - 100 %–100 % alcoholic solution was sequentially used to dehydrate for 20 min, and followed by 100 % acetone for 15 min. Subsequently, the resin blocks were prepared and cut into 60–80 nm slices. The sections of cell containing bacteria were placed on a 150-mesh copper mesh, and the morphology of intracellular/extracellular bacteria in macrophages was observed and photographed using transmission electron microscopy (TEM, HT7800/HT7700, HITACHI, Japan).

## 5.8. In vivo experiments

***Mouse subcutaneous implantation:*** Eight-week-old male C57BL/6 mice were selected to establish percutaneous implantation model. Then the mice in each group were anesthetized by intraperitoneal injection using 4 % chloral hydrate. The dorsal area of the mice was prepared and sterilized. After punching a 2 mm-diameter opening in the mouse's back using a 2 mm-diameter punch, the pre-prepared sample was inserted. Prior to usage, the samples of PEEK, SP, SPLA5, SPLA10, and SPLA20 were prepared by dipping one end of the sample into *S. aureus* suspension ($5 \times 10^6$ CFU/mL) and soaking it for 1 h at 37 °C. Then at 1 day, 4 days, and 14 days after surgery, the skins of the mice were harvested and subjected to a series of analytical processes.

***Histopathology and immunohistochemistry:*** The collected animal tissues were paraffin-embedded and cut into tissue slices. These slices were saved for further Giemsa staining, HE staining, Masson staining, immunohistochemistry staining, and immunofluorescence staining. Giemsa staining was used to mark infiltrating bacteria in tissue. HE staining was used to observe tissue healing and inflammatory cell infiltration. Masson staining and immunohistochemistry staining were

applied to visualize the distribution of collagen in the tissue. The paraffin section went through deparaffinization, rehydration, and washing for Giemsa, HE, and Masson staining. Wright's Giemsa staining kit (Servicebio, G1007), H&E Staining Kit (Servicebio, G1003), and Masson dye solution set (Servicebio, G1006) were used to stain the slices, respectively. Then the slices were further dehydrated and sealed for observation. For immunohistochemistry staining, rabbit polyclonal anti-Col-III antibody (Servicebio, GB111629, 1: 500) and rabbit polyclonal anti-Col-II antibody (Servicebio, GB11021, 1: 200), and secondary antibody, HRP-labeled goat anti-rabbit IgG (Servicebio, GB23303, 1: 200), were used to stain Col-III and Col-II, respectively. And specific primary antibodies, rabbit polyclonal anti-F4/80 antibody (Servicebio, GB113373, 1: 5000), rabbit polyclonal anti-iNOS antibody (Servicebio, GB11119, 1: 100), rabbit polyclonal anti-Arg-1 antibody (Servicebio, GB11285, 1: 3000), and secondary antibodies, CY3-labeled goat anti-rabbit IgG (Servicebio, GB21303, 1: 300), CY5-labeled goat anti-rabbit IgG (Servicebio, GB27303, 1: 400), Alexa Fluor 488 labeled goat anti-rabbit IgG (Servicebio, GB25303, 1: 400) were chose to label macrophages, M1 type, and M2 type, respectively. The experiments were carried out by Servicebio (Wuhan, China). Hamamatsu NanoZoomer S60 (Hamamatsu, Japan) and confocal laser scanning microscope (Pannoramic° MIDI, 3DHISTECH, Hungary) were utilized to monitor and capture photographs of the staining outcomes, which were then analyzed with ImagePro software.

***RNA sequence***: The collected animal tissues were immediately placed in lyophilization tubes and stored at −80 °C until further experiments. Total RNA was extracted using TRIzol reagent following the manufacturer's protocol. The NanoDrop 2000 spectrophotometer (Thermo Scientific, USA) was used to measure RNA purity and quantification. RNA integrity was then assessed using the Agilent 2100 Bioanalyzer (Agilent Technologies, USA). Afterward, the VAHTS Universal V6 RNA-seq Library Prep Kit was used to construct the cDNA libraries according to the manufacturer's protocol, and the libraries were then sequenced by the llumina Novaseq 6000. Differential expression gene (DEGs) were analyzed by the DESeq2. DEGs were defined by a threshold of foldchange $>2$ and q value $< 0.05$. Subsequently, KEGG pathway enrichment analysis was performed on DEGs to screen for key genes. The RNA sequence (RNA-seq) and analysis were carried out by OE Biotech Co., Ltd. (Shanghai, China).

***Western blot analysis***: The collected animal tissues were immediately placed in lyophilization tubes and stored at −80 °C. Western blot was used to quantify the C3 expression. Firstly, RIPA reagent was added to lyse the tissues. The lytic tissue solution was centrifuged at 12,000 rpm at 4 °C for 10 min and the supernatant was collected. Protein quantification was performed using BCA kit. The pretreated protein samples were separated by electrophoresis to prepare the bearer films of the target protein. Then, the above films were immersed in 5 % skim milk and incubated for 1 h, and the primary antibody rabbit monoclonal anti-C3 antibody (abcam, ab200999, 1: 2000) was added and incubated at 4 °C overnight. The films were incubated with secondary antibody peroxidase affinipure goat anti-rabbit IgG (H + L) (Jackson, 111-035-003, 1: 20000) after washed by tris buffered saline-tween 20 (TBST). β-actin was as the internal control. After washed by TBST, the blots could be visualized using ECL detection reagents (Thermo Fisher Scientific, USA). Image J software was used to analyze the results.

***Rat femur implantation***: Eight-week-old male SD rats were selected to establish the rat femoral defect models. Then the rats in each group were anesthetized by intraperitoneal injection using 4 % chloral hydrate. Next, the rat's knee area was completed skin preparation, and the skin in that surgical area was sterilized. The skin was then incised at the surgical site, bluntly separating the muscle tissue, and exposing the distal femur. After that, a hole (2 mm in diameter) was drilled in intercondylar fossa, parallel to the sagittal plane. Then 10 μL of *S. aureus* solution ($1 \times 10^4$ CFU/mL) was added, and the holes were filled with previously prepared samples of PEEK, SP, SPLA5, SPLA10, and SPLA20, respectively. Then at 4 weeks after surgery, the femurs of the rats were

harvested and subjected to a series of analytical processes.

***Micro-CT evaluation***: Micro-computed tomography (Micro-CT, SKYSCAN1076) was used to detect the new bone formation of SD rat femur with the parameters of 70 kV, 114 mA, resolution of 18.2 μm, and integration time of 250 ms. The new bone formed around the implanted sample was three-dimensionally reconstructed through a series of two-dimensional tomography images, and the region of interest was selected from the two-dimensional images for reconstruction analysis.

**Statistical Analysis**: GraphPad Prism (Version 9.0, GraphPad Software, USA) was used for data analysis. Quantitative data were expressed as mean $\pm$ standard deviation (SD). One-way ANOVA analysis, two-way ANOVA analysis and Tukey's multiple comparison tests were used to analyze the significant differences. $*p < 0.05$, $**p < 0.01$ $***p < 0.001$ and $****p < 0.0001$.

## Ethics approval and consent to participate

The experimental protocol concerning animals used in this work was approved by the Shanghai Tongren Hospital Ethics Committee (2021-090-01).

## CRediT authorship contribution statement

**Tong Zhao:** Writing – original draft, Visualization, Software, Methodology, Formal analysis, Data curation. **Xingdan Liu:** Writing – original draft, Visualization, Software, Methodology, Formal analysis, Data curation. **Zhuangzhuang Chu:** Data curation. **Jing Zhao:** Data curation. **Dongya Jiang:** Data curation. **Xiaohua Dong:** Data curation. **Ziyi Lu:** Data curation. **Kelvin W.K. Yeung:** Writing – review & editing, Funding acquisition. **Xuanyong Liu:** Writing – review & editing, Funding acquisition. **Liping Ouyang:** Writing – review & editing, Project administration, Funding acquisition, Conceptualization.

## Declaration of competing interest

Kelvin W. K. Yeung is an associate editor for *Bioactive Materials* and was not involved in the editorial review or the decision to publish this article. Xuanyong Liu is an editorial board member for *Bioactive Materials* and was not involved in the editorial review or the decision to publish this article. All authors declare that there are no competing interests.

## Appendix A. Supplementary data

Supplementary data to this article can be found online at https://doi.org/10.1016/j.bioactmat.2024.05.025.

## References

[1] N.G. Fischer, C. Aparicio, Junctional epithelium and hemidesmosomes: tape and rivets for solving the "percutaneous device dilemma" in dental and other permanent implants, Bioact. Mater. 18 (2022) 178–198.

[2] M.N. Abdallah, Z. Badran, O. Ciobanu, N. Hamdan, F. Tamimi, Strategies for optimizing the soft tissue seal around osseointegrated implants, Adv. Healthcare Mater. 6 (2017).

[3] Zhi Zheng, Pengjia Liu, Zhang Xingmin, Jingguo xin, Yongjie wang, Xiaosong Zou, Xiaohan Mei, Shuling Zhang, Shaokun Zhang, Strategies to improve bioactive and

antibacterial properties of polyetheretherketone (PEEK) for use as orthopedic implants, Mater. Today Bio. 16 (2022).

[4] Liping Ouyang, Baohui Chen, Xingdan Liu, Donghui Wang, Li Yang, Yun Liao, Kelvin W.K. Yeung, Xuanyong Liu, Puerarin@Chitosan composite for infected bone repair through mimicking the bio-functions of antimicrobial peptides, Bioact. Mater. 21 (2023) 520–530.

[5] Xingdan Liu, Haifeng Zhang, Bangcheng Yan, Kelvin W.K. Yeung, Yun Liao, Liping Ouyang, Xuanyong Liu, On-off phagocytosis and switchable macrophage activation stimulated with NIR for infected percutaneous tissue repair of polypyrrole-coated sulfonated PEEK, Adv. Sci. 10 (2022) 2205048.

[6] Xindan Liu, Liping Ouyang, Lan Chen, Yuqin Qiao, Xiaohan Ma, Gguohua Xu, Xuanyong Liu, Hydroxyapatite composited PEEK with 3D porous surface enhances osteoblast differentiation through mediating NO by macrophage, Regen. Biomater 9 (2022) rbab076.

[7] Liping Ouyang, Yaochao Zhao, Guodong Jin, Tao Lu, Li Jinhua, Yuqin Qiao, Congqin Ning, Xianlong Zhang, Paul K. Chu, Xuanyong Liu, Influence of sulfur content on bone formation and antibacterial ability of sulfonated PEEK, Biomaterials 83 (2016) 115–126.

[8] Steven M. Kurtz, John N. Devine, PEEK biomaterials in trauma, orthopedic, and spinal implants, Biomaterials 28 (2007) 4845–4869.

[9] Y. Zhao, H.M. Wong, W. Wang, P. Li, Z. Xu, E.Y. Chong, C.H. Yan, K.W. Yeung, P. K. Chu, Cytocompatibility, osseointegration, and bioactivity of three-dimensional porous and nanostructured network on polyetheretherketone, Biomaterials 34 (2013) 9264–9277.

[10] G. Weiss, U.E. Schaible, Macrophage defense mechanisms against intracellular bacteria, Immunol. Rev. 264 (2015) 182–203.

[11] Y. Duan, H. Chu, K. Brandl, L. Jiang, S. Zeng, N. Meshgin, E. Papachristoforou, J. Argemi, B.G. Mendes, Y. Wang, H. Su, W. Sun, C. Llorente, T. Hendrikx, X. Liu, M. Hosseini, T. Kisseleva, D.A. Brenner, R. Bataller, P. Ramachandran, M. Karin, W. Fu, B. Schnabl, CRIg on liver macrophages clears pathobionts and protects against alcoholic liver disease, Nat. Commun. 12 (2021) 7172.

[12] Houghton A. McGarry, William O. Hartzell, Clinton S. Robbins, Gomis-Ruth F. Xavier, D. Shapiro Shapiro, Macrophage elastase kills bacteria within murine macrophages, Nature 460 (2009) 637–641.

[13] Marie Wolf, Selene M. Clay, Siyu Zheng, Peipei Pan, Matilda F. Chan, MMP12 inhibits corneal neovascularization and inflammation through regulation of CCL2, Sci. Rep. 9 (2019) 11579.

[14] Tadie Jean Marc, Henno Priscilla, Leroy Ingrid, Danel Claire, Naline Emmanuel, Faisy Christophe, Riquet Marc, Levy Marilyne, Israel-Biet Dominique, Delclaux Christophe, Role of nitric oxide synthase/arginase balance in bronchial reactivity in patients with chronic obstructive pulmonary disease, Am. J. Physiol. Lung Cell Mol. Physiol. 294 (2008) L489–L497.

[15] X. Zheng, L. Xin, Y. Luo, H. Yang, X. Ye, Z. Mao, S. Zhang, L. Ma, C. Gao, Near-infrared-Triggered dynamic surface topography for sequential modulation of macrophage phenotypes, ACS Appl. Mater. Interfaces 11 (2019) 43689–43697.

[16] P.J. Murray, Macrophage polarization, Annu. Rev. Physiol. 79 (2017) 541–566.

[17] John Henderson, O'Reilly Steven, The emerging role of metabolism in fibrosis, Trend. Endocrin. Met. 32 (2021) 639–653.

[18] Z.H. Xiang, X.H. Guan, Z.F. Ma, Q. Shi, M. Panteleev, F.I. Ataullakhanov, Bioactive fibrous scaffolds with programmable release of polypeptides regulate inflammation and extracellular matrix remodeling, Regen. Biomater 10 (2023).

[19] R. Mata, Y. Yao, W. Cao, J. Ding, T. Zhou, Z. Zhai, C. Gao, The dynamic inflammatory tissue microenvironment: signality and disease therapy by biomaterials, Research 2021 (2021) 4189516.

[20] S. Saha, I.N. Shalova, S.K. Biswas, Metabolic regulation of macrophage phenotype and function, Immunol. Rev. 280 (2017) 102–111.

[21] B. Kelly, L.A. O'Neill, Metabolic reprogramming in macrophages and dendritic cells in innate immunity, Cell Res. 25 (2015) 771–784.

[22] S.K. Wculek, G. Dunphy, I. Heras-Murillo, A. Mastrangelo, D. Sancho, Metabolism of tissue macrophages in homeostasis and pathology, Cell. Mol. Immunol. 19 (2022) 384–408.

[23] S.E. Weinberg, L.A. Sena, N.S. Chandel, Mitochondria in the regulation of innate and adaptive immunity, Immunity 42 (2015) 406–417.

[24] E.L. Mills, B. Kelly, A. Logan, A.S.H. Costa, M. Varma, C.E. Bryant, P. Tourlomousis, J.H.M. Dabritz, E. Gottlieb, I. Latorre, S.C. Corr, G. McManus, D. Ryan, H.T. Jacobs, M. Szibor, R.J. Xavier, T. Braun, C. Frezza, M.P. Murphy, L.A. O'Neill, Succinate dehydrogenase supports metabolic repurposing of mitochondria to drive inflammatory macrophages, Cell 167 (2016) 457–470 e413.

[25] Christopher Hoyle, P. Green Jack, Stuart M. Allan, David Brough, Lemarchand Eloise, Itaconate and fumarate derivatives inhibit priming and activation of the canonical NLRP3 inflammasome in macrophages, Immunology 165 (2022) 460–480.

[26] P.S. Liu, H. Wang, X. Li, T. Chao, T. Teav, S. Christen, G. Di Conza, W.C. Cheng, C. H. Chou, M. Vavakova, C. Muret, K. Debackere, M. Mazzone, H.D. Huang, S. M. Fendt, J. Ivanisevic, P.C. Ho, alpha-ketoglutarate orchestrates macrophage activation through metabolic and epigenetic reprogramming, Nat. Immunol. 18 (2017) 985–994.

[27] Shan Cao, Li Yixuan, Song Rui, Meng Xianyi, Maximilian Fuchs, Chunguang Liang, Kachler Katerina, Meng Xinyu, Jinming Wen, Schlötzer-Schrehardt Ursula, Taudte Verena, Gessner Arne, Kunz Meik, Schleicher Ulrike, Mario M. Zaiss, Kastbom Alf, Xiaoxiang Chen, Schett Georg, Bozec Aline, L-arginine metabolism inhibits arthritis and inflammatory bone loss, Ann. Rheum. Dis. 83 (2024) 72–87.

[28] Li Jiaying, Jinjin Ma, Heng Sun, Yu Meizhe, Huan Wang, Meng Qingchen, Li Zexi, Dachuan Liu, Jianzhong Bai, Guoping Liu, Xiaodong Xing, Fengxuan Han, Li Bin, Transformation of arginine into zero-dimensional nanomaterial endows the material with antibacterial and osteoinductive activity, Sci. Adv. 9 (2023).

[29] X. Wang, W. Lv, J. Xu, A. Zheng, M. Zeng, K. Cao, X. Wang, Y. Cui, H. Li, M. Yang, Y. Shao, F. Zhang, X. Zou, J. Long, Z. Feng, J. Liu, Hepatic suppression of mitochondrial complex II assembly drives systemic metabolic benefits, Adv. Sci. 9 (2022) e2105587.

[30] J. Van den Bossche, L.A. O'Neill, D. Menon, Macrophage immunometabolism: where are we (going)? Trends Immunol. 38 (2017) 395–406.

[31] S.A. Eming, P.J. Murray, E.J. Pearce, Metabolic orchestration of the wound healing response, Cell Metabol. 33 (2021) 1726–1743.

[32] Y. Wang, P. Deng, Y. Liu, Y. Wu, Y. Chen, Y. Guo, S. Zhang, X. Zheng, L. Zhou, W. Liu, Q. Li, W. Lin, X. Qi, G. Ou, C. Wang, Q. Yuan, Alpha-ketoglutarate ameliorates age-related osteoporosis via regulating histone methylations, Nat. Commun. 11 (2020) 5596.

[33] G.A. Timblin, K.M. Tharp, B. Ford, J.M. Winchester, J. Wang, S. Zhu, R.I. Khan, S. K. Louie, A.T. Iavarone, J. Ten Hoeve, D.K. Nomura, A. Stahl, K. Saijo, Mitohormesis reprogrammes macrophage metabolism to enforce tolerance, Nat. Metab. 3 (2021) 618–635.

[34] J. Foster Timothy, Immune evasion by staphylococci, Nat. Rev. Microbiol. 3 (2005) 948–958.

[35] Francisco J. Fernández, Jorge Santos-López, Martínez-Barricarte Rubén, Querol-García Javier, Martín-Merinero Héctor, Navas-Yuste Sergio, Savko Martin, William E. Shepard, de Córdoba Santiago Rodríguez, Vega M. Cristina, The crystal structure of iC3b-CR3 αI reveals a modular recognition of the main opsonin iC3b by the CR3 integrin receptor, Nat. Commun. 13 (2022).

[36] Li Yang, Dan Zhang, Li Wenjing, Hongbing Lin, Chendi Ding, Qingyun Liu, Liangliang Wang, Li Zimu, Mei Lin, Hongzhong Chen, Yanli Zhao, Xiaowei Zeng, Biofilm microenvironment triggered self-enhancing photodynamic immunomodulatory microneedle for diabetic wound therapy, Nat. Commun. 14 (2023).

[37] Yusen Qiao, Yu Lei, Peng Yang, Miao Chen, Haifu Sun, Lingjie Wang, Bangzhao Wu, Chun-do Oh, Huilin Yang, Jiaxiang Bai, Geng Dechun, Spatiotemporal immunomodulation and biphasic osteo-vascular aligned electrospun membrane for diabetic periosteum regeneration, Adv. Sci. 10 (2023) e2302874.

[38] Long Jing, Yao Zhenyu, Wei Zhang, Ben Liu, Kaiming Chen, Li Long, Teng Bin, Xiang-Fu Du, Li Cairong, Xue-Feng Yu, Ling Qin, Lai Yuxiao, Regulation of osteoimmune microenvironment and osteogenesis by 3D-printed PLAG/black phosphorus scaffolds for bone regeneration, Adv. Sci. 10 (2023) e2302539.